❒ 677

A battery integrated multiple input DC-DC boost converter

Azuka Affam[1], Yonis M. Yonis Buswig[1], Al-Khalid Hj Othman[1], Norhuzaimin Julai[1], Hani Albalawi[2,3]
[1]Department of Electrical and Electronic Engineering, Faculty of Engineering, Universiti Malaysia Sarawak, Kota Samarahan, Malaysia
[2]Department of Electrical Engineering, University of Tabuk, Tabuk, Saudi Arabia
[3]Renewable Energy and Energy Efficiency Center (REEC), University of Tabuk, Tabuk, Saudi Arabia

Article Info

ABSTRACT

In this paper, the proposed single boost converter aims to harness more than one renewable energy (RE) input source and achieve a high voltage gain. The interleaved technique combined with voltage multiplier (VM) cells, reduced inductor current and attained high voltage transfer ratio. The boost converter possesses two unidirectional input ports and a bidirectional input port that is connected to a battery storage. The duty ratios of the power and interleaving switches are used to regulate the output voltage of the proposed converter. Three operation modes are identified, and steady state analyses of the converter are presented and discussed. The converter can store excess energy in the battery during periods of abundance and deliver power to the loads when the RE sources are low or unavailable. In addition, the output voltage is higher than that of the conventional boost converter. The converter delivered 278 V from 12 V and 24 V dual input sources. The converter operation is simulated and verified using MATLAB/Simulink.
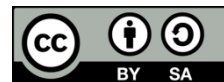
Corresponding Author:

Azuka Affam
Department of Electrical and Electronic Engineering, Faculty of Engineering, Universiti Malaysia Sarawak
Kota Samarahan, Sarawak, Malaysia
Email: 18010014@siswa.unimas.my

1. INTRODUCTION

Environmental degradation and predicted depletion of fossil fuels have been a source of concern about employing sustainable and clean energy sources for power generation. The quest for clean energy resources extends to the transportation sector [1]. Electric cars are expected to summarily replace gasoline or diesel-powered cars soon as a way to mitigate environmental pollution [2]. Recently, renewable energy (RE) sources like fuel cells (FC), wind turbines and photovoltaic (PV) cell have been utilized in hybrid electric vehicles [3], microgrids [4], traffic lights [5], or telecommunication/satellite systems [6].

The RE sources fall short in performance due to occasional unavailability, low output voltage levels, and limited slew rates [7]. The limited slew rate is common with FC and some storage devices like supercapacitors and batteries. An example of the stochastic nature of RE sources is the inability of PV cells to deliver at night or during low irradiance [8]. Other examples are wind turbines and hydrokinetic turbines that may experience insufficient wind speed and low water velocity respectively.

An approach to solving the problems of irregularity and slew rate posed by RE sources is to combine two or more of these energy sources to deliver regulated output to the load. Traditionally, separate DC-DC converters have been used for each RE source with outputs connected to a common DC bus [9]. This configuration is bulky and expensive with complex communication control requirements. Contemporary multiple input converters have advantages of reduced size, easier control and lower number of components thereby being cheaper [10]. A group of RE sources serving a load via a single multiple input converter. In this case, the respective RE sources are routed to the multiple input converter [11]. This converter can

process and regulate the source voltages thus delivering power to the load. In this way, the restrictions posed by the traditional multiple input converter are successfully eliminated.

General methods of synthesizing non-isolated multi-input converters (MICs) have been proposed [12], [13]. Liu and Chen [12] used an approach based on using appropriate connections to add extra pulsating voltage or current source to the pulse width modulation (PWM) converter. Li *et al.* [14] developed a set of rules based on the breakdown of the prime converter pulsating current source cells (PCSC). These rules lead to two families of MICs. The low voltage gains of the converters proposed in these papers imply their poor performance in systems that require high voltage.

A multi input switched capacitor based converter is introduced [15]. This topology eliminates the need for the inductor. The energy transfer is done by the capacitors and switches. This configuration suffers from high output ripple and output leakage voltage. Coupled inductor have been used to achieve high gain in [16], [17]. The coupled inductors suffer from some leakage inductance. High voltage gain has been achieved by using voltage multiplier (VM) cells [18]. The VM stages are positioned after a primary boost converter. The design lacks a bidirectional function for a storage element. The large number of passive components result in the high dissipation loss.

A modular non-coupled inductor based bidirectional multi input converter is proposed [19]. Several SISO converters with non-coupled inductors can share a common filter and bidirectional switch. The non-coupled converters are positioned in an interleaved structure. Reduced normalized voltage stress and very high voltage gain are the advantages of this converter. However, the aim of sharing components is not achieved. The driving circuits for control imply are complex. In addition, the component count increases with the addition of an extra input source.

The modified single-ended primary-inductor converter (SEPIC) converter [20] has a third energy storage input. In this converter, the input sources can charge the battery and at the same time, deliver power to the load in one operation mode. The battery can also complement the input sources when there is insufficient power to the load. The major weakness of this converter is the low voltage gain. The three input DC-DC converter has been adapted for PV, fuel cell and battery inputs [21], [22]. There are two unidirectional ports and one bidirectional port. The duty rations of switches are used to control the converter to give power to the load, and charge or discharge the battery simultaneously or individually. The voltage gain is slightly more when compared to conventional converters. There is a high number of passive elements. This reduces efficiency due to dissipation loss.

A dual input interleaved converter was proposed [23]. High efficiency is achieved by implementing zero voltage switching (ZVS) through an auxiliary circuit. Low voltage gain and high number of power switches stand as disadvantages to this converter. Another interleaved topology has two inputs, one PV source and a battery storage [24]. The converter can be extended to multiple outputs by using parallel switches. Although there is a bidirectional port, the voltage gain of the converter is low, and it cannot accommodate more than one RE source. A multiple input multi-level output converter was proposed in [25]. The simple configuration boasts of low number of passive elements and high voltage gain. However, this converter has an unusually high number of switches. This short coming has been tackled by inserting diodes in [26] thereby achieving lower switch count.

In this paper, a battery integrated interleaved multiple input DC-DC boost converter is proposed. The state of the art presented so far shows that there is need to accommodate more RE sources as well as achieve higher output voltage. The proposed converter can interface two RE sources and an energy storage device. The converter can reduce the inductor current as well as delivering a high step up to the input voltage. This paper is organized as follows. The first section provides the background and literature review. The second section presents the proposed converter, operation modes and circuit analysis. Simulation results and comparisons are presented and discussed in the third section. Conclusions are drawn in the fourth section.

2.   CONVERTER TOPOLOGY

In this section, the proposed converter topology is introduced along with the operation modes and circuit analysis. The proposed structure is presented in Figure 1. Three distinct sections of the converter can be identified. The input section, interleaving section and the VM section. The input section has three input sources, V_1, V_2 and V_b V_1 and V_2 are unidirectional ports. V_b is a bidirectional port hence it is ideal for connection to a storage element. The converter has $n + 3$ power switches. A pulsating voltage source cell (PVSC) is formed by V_1, switch S_1 and diode D_1. Two additional PVSCs are formed by V_2, S_2, D_2 and V_b, S_3, D_3 respectively. Control of the unidirectional ports V_1 and V_2 can be done by manipulating the duty ratios, d_1 and d_2, of switches S_1 and S_2. Switches S_3 and S_4 facilitates the bidirectional capability of V_b. Battery discharging can be done by controlling the duty ratio d_2 of S_3 while the duty ratio d_4 of switch S_4 controlled the charging of the battery. In the interleaving section, inductors, L_1 and L_2, are connected in an interleaved

manner with switches S_5 and S_6. The VM section has a combined single stage of VM cell with capacitors C_1, C_2 and diodes D_4-D_6. C_{out} and D_{out} are the respective output capacitor and diode. R_L is the load served by output voltage, V_o.
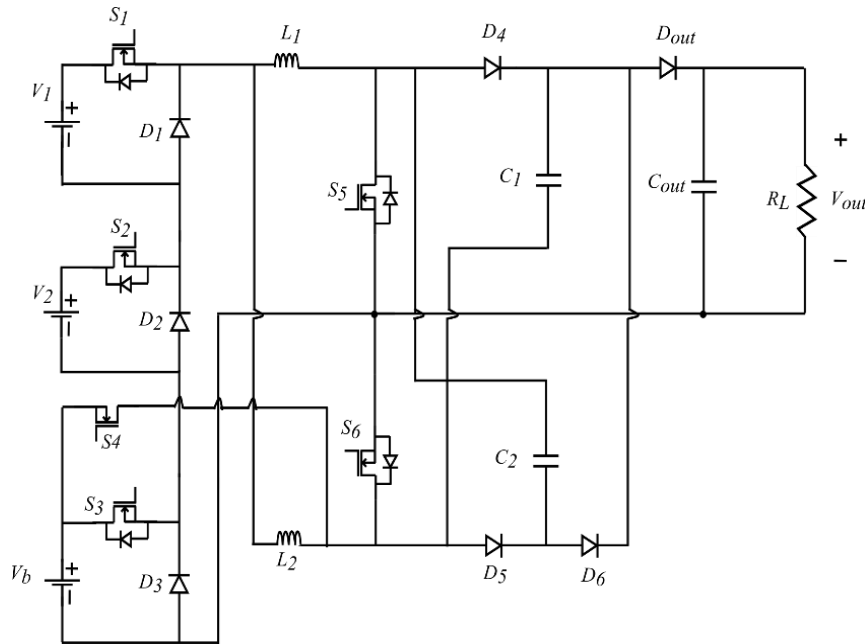

Figure 1. Proposed battery integrated multiple input boost converter

2.1. Operation mode one

In this mode, the battery state of charge is optimal and the power of input sources V_1 and V_2 can sufficiently serve the load. During this operation mode, the battery neither charges nor discharges. This is the default operation mode. In this mode S_3 and S_4 are permanently turned off. The switching sequence in this operation mode is explained as follows:

a. Switching mode 1 $[0 < t < D1T]$: the circuit is represented in Figure 2(a). Switches S_1, S_2, S_5, and S_6 are turned on. Input source, the sum of V_1 and V_2 charges inductors L_1 and L_2. Diode D_3 is forward biased and all other diodes are reverse biased. Capacitors C_1 and C_2 are idle. C_{out} delivers power to the load.

b. Switching mode 2 $[D_1T < t < D_2T]$: the circuit is illustrated in Figure 2(b). During this switching interval, switch S_2 continues conducting while S_1 is turned off. Only V_2 can deliver energy at this time. Similarly, interleaving switch S_5 is turned off and S_6 continues conducting. D_6 is forward biased. L_1 and C_2 charge capacitor C_1. C_{out} serves the load.

c. Switching mode 3 $[D_2T < t < D_3T]$: the circuit is shown in Figure 2(c). S_2 is turned off and S_1 is turned on. S_5 and S_6 are turned on. V_1 charges L_1 and L_2. C_1 and C_2 are idle. C_{out} services the load.

d. Switching mode 4 $[D_3T < t < T]$: S_1 and S_2 are turned on, S_5 remains on, S_6 is turned off. L_1 continues charging by V_1 and V_2. L_2 and C_1 discharge to the load. C_2 is charging. Figure 2(d) depicts the circuit. Based on Figures 2(a)-(d) and applying the voltage-second balance principle on the inductors and the ampere-second balance principle on the capacitors, in (1)-(4) can be obtained.

$$L_1: (V_1 + V_2)D_1T + (V_2 + V_{c2} - V_{c1})(1 - D_3)T = 0 \tag{1}$$

$$L_2: (V_1 + V_2)D_1T + ((V_1 + V_2) + V_{c1} - V_o)(1 - D_3)T = 0 \tag{2}$$

$$C_1: (iL_1 + iC_2)(D_2 - D_1)T - (iL_2 - i_o)(1 - D_3)T = 0 \tag{3}$$

$$C_2: iL_2(1 - D_3)T - (iL_1 - iC_1)(D_2 - D_1)T = 0 \tag{4}$$

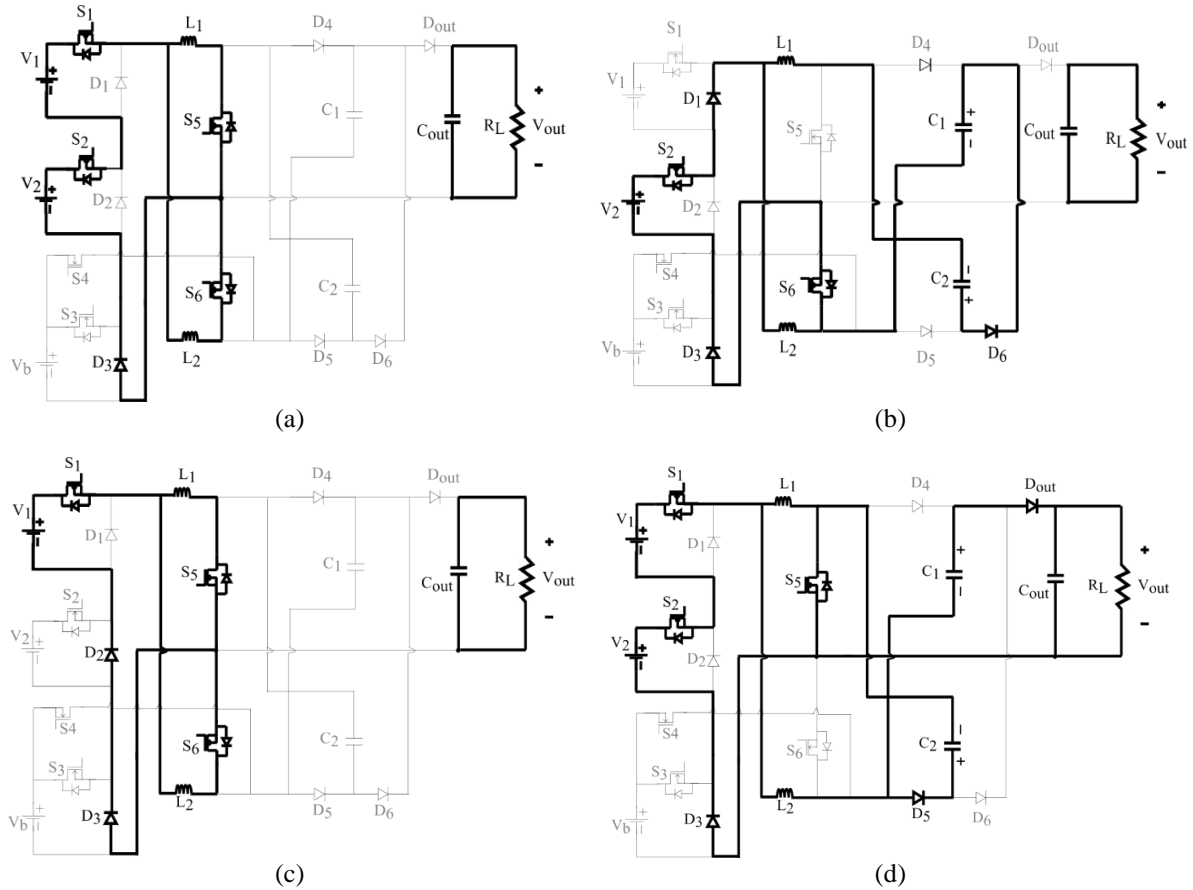$$i_{batt} = 0, P_{batt} = 0 \tag{5}$$

Figure 2. Current paths for the first operation mode of proposed converter (a) switching mode 1,
(b) switching mode 2, (c) switching mode 3, and (d) switching mode 4

2.2. Operation mode two

This operation mode occurs when the RE sources are incapable of servicing the load optimally. In this condition, the attached battery storage device, V_b steps in to augment the power delivery from the RE sources to the load. Switch S_3 plays the role of allowing or disallowing the battery to deliver power to the load. S_4 remains turned off during this operation mode. The respective switching modes are described as:

a. Switching mode 1 $[0 < t < D_1T]$: the circuit is represented in Figure 3(a). Switches S_1, S_2, S_3, S_5 and S_6 are turned on. Input sources, V_1, V_2 and V_b charge inductors L_1 and L_2. Capacitors C_1 and C_2 are idle and all diodes are reverse biased. C_{out} delivers power to the load.

b. Switching mode 2 $[D_1T < t < D_2T]$: this switching mode is the same as switching mode 2 of the first operation mode.

c. Switching mode 3 $[D_2T < t < D_3T]$: the circuit is shown in Figure 3(b). V_1 and V_b charge L_1 and L_2 though the conduction of the S_1, S_3 and S_5 and S_6 respectively. C_{out} serves the load.

d. Switching mode 4 $[D_3T < t < T]$: V_1, V_2 and V_b deliver power to the converter through S_1, S_2 and S_3 respectively. L_1 is charged through S_5. C_2 is charging and C_1 discharges. L_2 delivers power to the load. The circuit is illustrated in Figure 3(c).

By applying the voltage-second balance principle on the inductors, in (6)-(9) can be obtained. The ampere-second balance principle on the capacitors gives the same as in all operation modes. This is because the switching pattern exist for all conditions of the interleaving switches.

$$L_1: (V_1 + V_2 + V_b)D_1T + (V_1 + V_2 + V_b)(1 - D_3)T = 0 \tag{6}$$

$$L_2: (V_1 + V_2 + V_b)D_1T + ((V_1 + V_2 + V_b) + V_{c1} - V_o)(1 - D_3)T = 0 \tag{7}$$

$$i_{batt} = (iL_1 + iL_2)(1 - D_3) \tag{8}$$

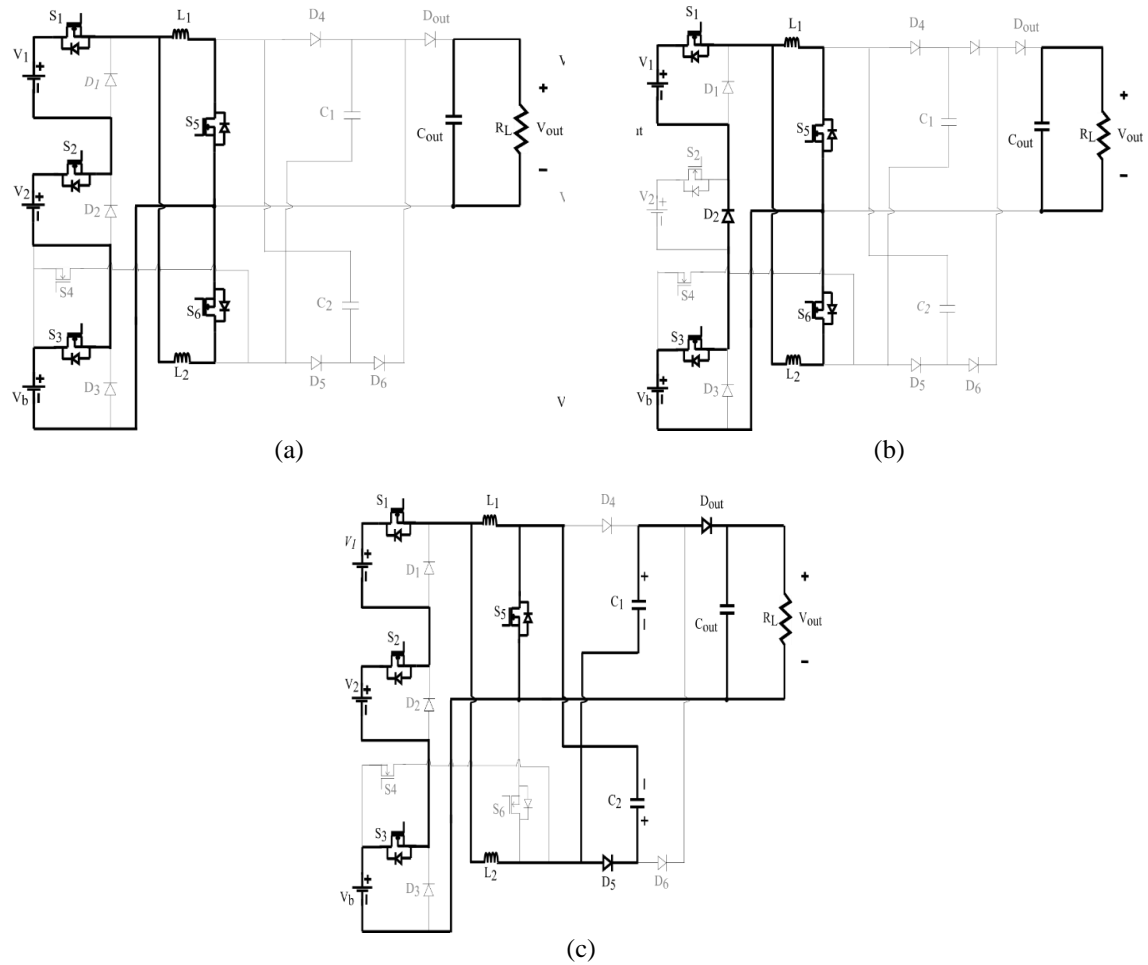$$P_{batt} = V_b(iL_1 + iL_2)(1 - D_3) \tag{9}$$

(a)

(b)

(c)

Figure 3. Current paths for the second operation mode of proposed converter (a) switching mode 1,
(b) switching mode 3, and (c) switching mode 4

2.3. Operation mode three

During this operation mode, the battery state of charge is depleted and the RE sources can service the load in addition to charging the battery. Switch S_4 plays the role of allowing charging current to the battery. S_3 remains turned off during this operation mode. The respective switching modes are described as:

a. Switching mode 1 $[0 < t < D1T]$: the switching mode is the same as the first switching mode of the first operation mode. Switch S_4 is turned off hence the battery is not charging.

b. Switching mode 2 $[D1T < t < D2T]$: S_2, S_4 and S_5 are turned on. L_1 is charged by V_2. The battery is charged from L_2 at this time. C_2 is charged through D_6 by L_1 and C_1. The output capacitor delivers power to the load. This is illustrated in Figure 4(a).

c. Switching mode 3 $[D2T < t < D3T]$: the circuit is shown in Figure 4(b). S_1, S_4, S_5, and S_6 are turned on. L_1, L_2 and V_b are charged by V_1. The capacitors are idle. D_4-D_6 are reverse biased. Power is delivered to the load by the output capacitor, C_{out}.

d. Switching mode 4 $[D3T < t < T]$: S_4 is turned off. This switching mode is the same as the switching mode of the first operation mode. No charging current enters the battery.

The switching patterns and inductor waveforms for the first operation mode, second operation mode and third operation mode are presented in Figures 5(a)-(c) respectively. It reveals that the same switching pattern are maintained for the respective switches, S_1, S_2, S_5 and S_6 in all the operation modes. It is different for switches, S_3 and S_4 because they function only during battery charging and discharging operation as can be seen from Figure 5(b) and Figure 5(c). In compliance with the switching pattern, the inductor current i_{L2} rises during the first three switching periods, t₀-t₃, and falls during the fourth switching period t₃-t₄. This is different for the current waveform of inductor i_{L1} which rises in the first switching period, falls during the second switching period, and resumes rising during the third and fourth switching periods. By applying the voltage-second balance principle on the inductors, in (10)-(13) can be obtained.

$$L_1: (V_1 + V_2)D_1T + (V_1 + V_2)(1 - D_3)T = 0 \qquad (10)$$

$$L_2: (V_1 + V_2)D_1T + ((V_1 + V_2) + V_{c1} - V_o)(1 - D_3)T = 0 \qquad (11)$$

$$i_{batt} = iL_2(D_3 - D_1) \qquad (12)$$
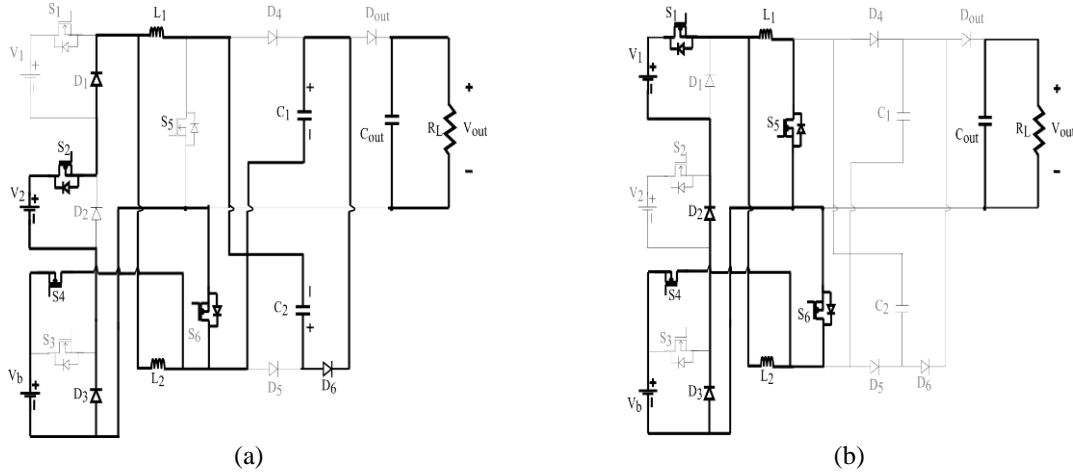
$$P_{batt} = V_b((iL_2(D_3 - D_1))) \qquad (13)$$

(a)   (b)

Figure 4. Current paths for the third operation mode of proposed converter (a) switching mode 2 and (b) switching mode 3
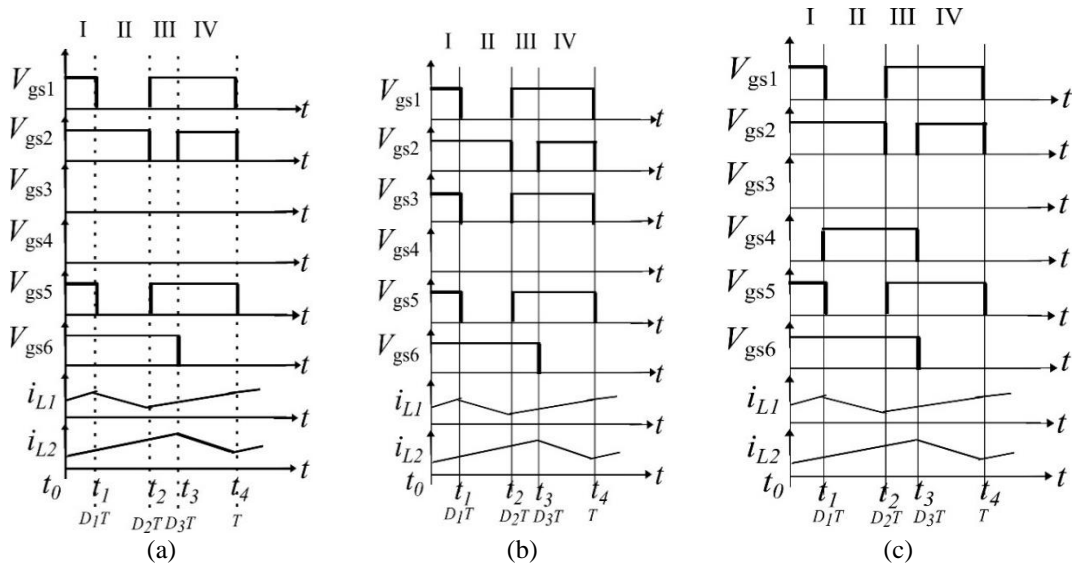

(a)   (b)   (c)

Figure 5. Switching pattern and inductor current waveform for operation modes (a) operation mode one, (b) operation mode two, and (c) operation mode three

2.4. Converter analysis and design

In analysis of the steady-state obtained for the proposed converter, the voltage of the capacitors, C_1 and C_2 can be obtained. Based on the switching mode of the upper interleaving switch, S_5 in Figure 2(b), the capacitor voltages can be expressed as (14):

$$V_{c1} - V_{c2} = \frac{V_2}{(1 - D_3)} \qquad (14)$$

Referring to the circuit for the lower interleaving switch, S_6 in Figure 2(d), the voltage across the capacitor V_{c2} is (15) and (16):

$$V_{c2} = \frac{V_1+V_2}{(1-D_3)} \tag{15}$$

$$V_o - V_{c1} = \frac{V_1+V_2}{(1-D_3)} \tag{16}$$

Substituting the duty ratio of the interleaved switches, the voltage across the capacitor, V_{c1} can be derived as (17) and (18):

$$V_{c1} = \frac{V_1+2V_2}{(1-D_3)^2} \tag{17}$$

from (2),

$$V_o = \frac{V_{c1}d_1}{(1-D_3)} \tag{18}$$

Combining (17) and (18), and including the duty ratios of the respective voltage sources, the output voltage of the first operation mode is calculated by (19):

$$V_o = \frac{V_1 d_1+2V_2 d_2}{(1-D_{5,6})^3} \tag{19}$$

The output voltage of the second operation mode is given by (20):

$$V_o = \frac{V_1 d_1+2V_2 d_2+V_b d_3}{(1-D_{5,6})^3} \tag{20}$$

where, $D_{5,6}$ is the duty ratio of the interleaved switches, S_5 and S_6, d_1, d_2, and d_3 are the duty ratios of S_1, S_2, and S_3 respectively.

For component selection, the interleaved inductors have the same inductance. The inductance can be calculated by (21):

$$L_1 = L_2 = \frac{V_{intotal}D_{5,6}}{f_{sw}\Delta i_L} \tag{21}$$

Where f_{sw} is the switching frequency; $V_{intotal}$ is the sum of all input voltages; and Δi_L is the change in inductor current.

The design of the capacitors is dependent on the tolerable AC ripples for the respective capacitor voltages. Hence the capacitor value can be calculated by (22):

$$C = \frac{I_c}{f_{sw}\Delta V} \tag{22}$$

3. RESULTS AND DISCUSSION

In this section, the parameter selection of the simulated converter will be presented. In addition, graphical illustrations of the results for specific operation modes and parameters will be presented and discussed. These will verify that the proposed converter meets the objective of accommodating more than one RE source alongside an energy storage device. In the latter part, some properties of proposed converter will be compared with other similar works. The properties to be compared include the number of input ports, bidirectional capability, number of semiconductor devices, and total number of components. Such comparisons will highlight the suitability of the proposed converter among other converters.

3.1. Simulation results

In a bid to confirm the compliance of the proposed converter with the discussed operation and characteristics, it has been simulated on the MATLAB/Simulink environment. The component sizes and other parameters are presented in Table 1. The values of the input voltages are 24 V, 12, and 12 V for V_1, V_2 and V_b respectively. The inductor value of 360 µH for each inductor are obtained using (19) with the desired current ripple. The switching frequency is 50 kHz. The duty ratio of the interleaving switches, S_5 and S_6 is 0.5 while

0.75 is used for the individual power switches, S_1 and S_2. In the first operating mode, the maximum input voltage delivered by V_1 and V_2 is 33 V. Figure 6 shows the state-of-charge (SOC) of the battery and the voltage levels of V_1 and V_2 during this operation mode. The battery SOC is 100% and does not deplete while V_1 and V_2 are 24 V and 12 V. The output voltage is 278 V with a load resistance of 500 Ω. The average values of the inductor currents, i_{L1} and i_{L2} are 5.1 A and 3.5 A respectively. The inductor current ripple, Δi_L is set at 1 A.

The inductor currents are illustrated in Figure 7. It can be observed that i_{L2} is higher than i_{L1}. This is because the number of VM is even and more current is drawn during the charging and discharging stages in L_2. Also, the waveforms of i_{L2} and i_{L1} appears inverted to relative to one another because there exists a phase delay between the switching signals. The voltage across the capacitors is shown in Figure 8. The maximum voltage across V_{c1} is 192 V while that of V_{c2} is 85.42 V. The voltage stress on the interleaving switches at 250 W is shown in Figure 9(a). The maximum voltage stress on S_5 and S_6 was 109.25 V and 86.82 V respectively. This brings to the fore, one advantage of VM cells being their ability to reduce voltage stress on the switch.

Table 1. Simulation parameters

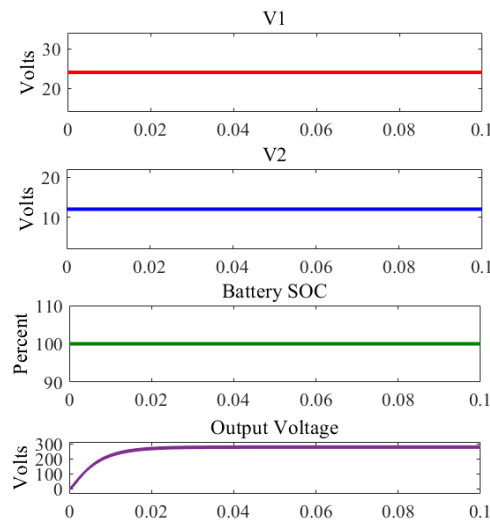| Component	Value
Input voltage	V_1=24 V, V_2=12 V, V_b=12 V
Switching frequency	F=50 kHz
Load resistance	R_L=500 Ω
Duty ratio	d_1, d_2, d_3=0.75, d_4, $d_{5,6.}$=0,5
Inductors	L_1=L_2=360 μH
Capacitors	C_1=C_2=20 μF, C_{out}=220 μF

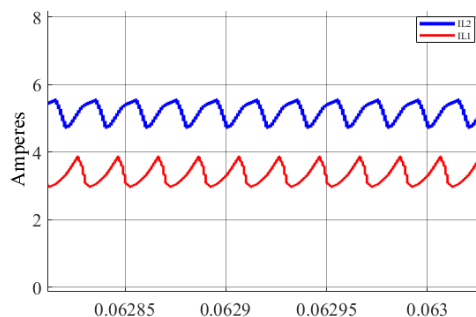Figure 6. Input voltage and battery SOC levels during operation mode one

Figure 7. Inductor currents

The voltage stress of the VM diodes and the output diode are shown in Figure 9(b). D_4 has the highest stress 278 V. This is equivalent to the output voltage and is because it is always in blocking mode

during the entire operation of the converter. D_5 and D_6 have a voltage stress of 192 V. This implies that the voltage stress on D_5 and D_6 is V_{c1}.
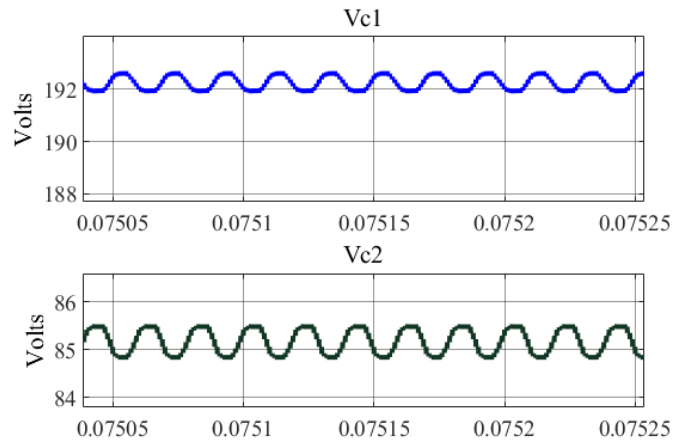

Figure 8. Maximum voltage across VM capacitors

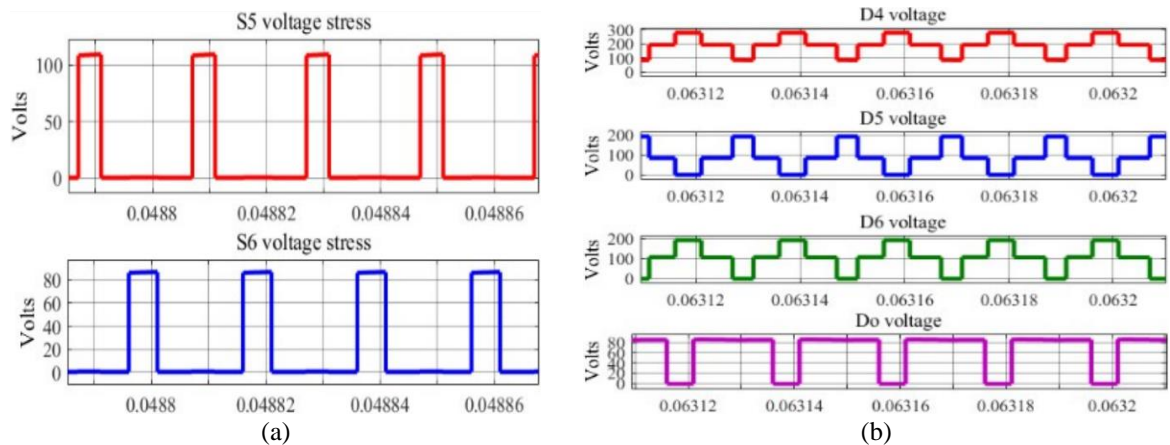|	
(a)	(b)

Figure 9. Voltage stress (a) switches and (b) diodes

In the simulation of the second operation mode, input sources V_1 and V_2 are assumed to be depleted hence the battery is called into action. The values for V_1, V_2 and V_b are 18 V, 6 V, and 12 V respectively. The maximum input voltage from all three supplies is 33 V. Since the interleaved switches adopt the same switching pattern in all the operation modes, the inductor currents, voltage stress and capacitor voltage and waveforms are almost the same as the first operation mode. Figure 10(a) shows the voltage output of V_1, V_2 and the SOC of the battery. The battery SOC reduces in the process of complementing V_1 and V_2. The output voltage is 275.5 V.

The input voltage levels, battery SOC, and converter output voltage in the third operation mode is presented in Figure 10(b). V_1 and V_2 are 24 V and 12 V respectively. The initial battery SOC is 50%. This SOC, slowly increased during operation to indicate battery charging in this mode. The output voltage of the third operation mode is 278 V. This is less than the first and second modes because the battery draws current for charging. The duty cycle of switch S_4 determine the charging rate of the battery. Increasing this duty cycle implies less power delivery to the converter and more charging current to the battery.

3.2. Comparison with other works

Comparing the proposed converter with previous works, the converter in [24] has lower voltage gain than this converter. In addition, the proposed converter has one more unidirectional input than [24]. While the converter in [27] boasts of high output voltage, the proposed converter has an advantage of capacity to

accommodate multiple input sources. This is an important factor in RE applications. The converter in [18] can function in RE applications because it has two unidirectional inputs and high output voltage. However, the proposed converter has an advantage of a bidirectional input that can store excess energy. It should be noted that the converters in [18], [27] higher output voltage because they have greater number of VM cell than the proposed converter. Table 2 shows comparisons between the properties of the proposed converter and other structures.
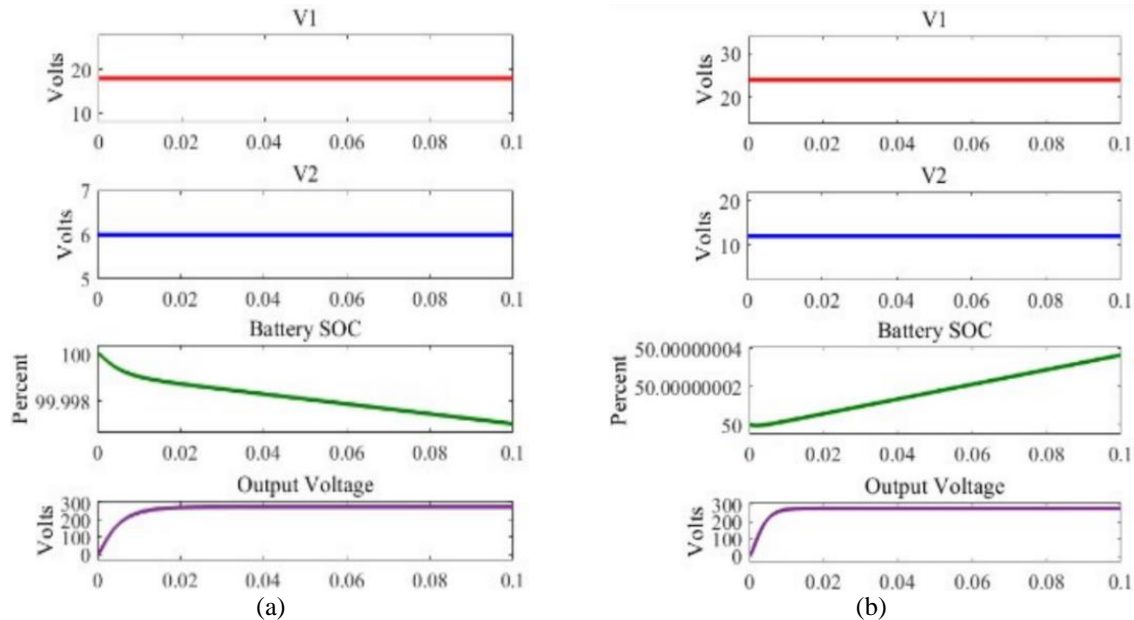
Figure 10. Input voltage and battery SOC levels (a) operation mode two and (b) operation mode three

Table 2. Comparison between proposed converter and previous works

Property	This work	[18]	[24]	[25]
Number of input ports	3	2	2	2
Number of switches	6	2	4	2
Inductor count	2	2	2	2
Diode count	7	5	7	5
Capacitor count	3	5	2	5
Total component count	18	14	15	14
Bidirectional port	Yes	No	Yes	No
Output voltage, Vo	$\dfrac{V_1 d_1 + 2V_2 d_2}{(1 - D_{5,6})^3}$	$\dfrac{3V_1}{1 - d_1} + \dfrac{2V_2}{1 - d_2}$	$\dfrac{V_{in}}{1 - D}$	$\dfrac{-5V_{in}}{1 - D}$

4. CONCLUSION

In this paper, the proposed multi-input converter achieved high output voltage in an interleaved inductor topology by taking advantage of two VM cells placed after the interleaving stage. The converter can provide energy from three sources. There are two unidirectional input ports and a bidirectional input port that is suitable for a battery storage. The individual energy sources can be controlled by their respective power switches. The battery storage port is a major advantage of the proposed converter. Excess energy from RE sources can be stored in the battery. On occasions of inadequate power, this stored energy can be channeled to satisfy the power requirements. The charge and discharge rate of the bidirectional port is dependent on the duty ratio of the power switch. Thus, the proposed converter is appropriate for use in RE applications. Future work will focus on developing an optimal control strategy for the converter.

REFERENCES

[1] A. Affam, Y. M. Buswig, A.-K. B. H. Othman, N. bin Julai, and O. Qays, "A review of multiple input DC-DC converter topologies linked with hybrid electric vehicles and renewable energy systems," *Renewable and Sustainable Energy Reviews*, vol. 135, pp. 1–23, Jan. 2021, doi: 10.1016/j.rser.2020.110186.

[2] K. J. Reddy and S. Natarajan, "Energy sources and multi-input DC-DC converters used in hybrid electric vehicle applications–A review," *International Journal of Hydrogen Energy*, vol. 43, no. 36, pp. 17387–17408, Sep. 2018, doi: 10.1016/j.ijhydene.2018.07.076.

[3] F. Akar, Y. Tavlasoglu, E. Ugur, B. Vural, and I. Aksoy, "A bidirectional nonisolated multi-input DC-DC converter for hybrid energy storage systems in electric vehicles," *IEEE Transactions on Vehicular Technology*, vol. 65, no. 10, pp. 7944–7955, Oct. 2016, doi: 10.1109/TVT.2015.2500683.

[4] F. Akar, Y. Tavlasoglu, and B. Vural, "Analysis and experimental verification of a multi-input converter for DC microgrid applications," *IET Power Electronics*, vol. 11, no. 6, pp. 1009–1017, May 2018, doi: 10.1049/iet-pel.2017.0456.

[5] J.-H. Park and J.-K. Kim, "A non-isolated dual-input DC-DC converter with wide input voltage range for renewable energy sources," in *2017 IEEE 3rd International Future Energy Electronics Conference and ECCE Asia (IFEEC 2017-ECCE Asia)*, Jun. 2017, pp. 654–658, doi: 10.1109/IFEEC.2017.7992116.

[6] K. Yari, S. H. Shahalami, and H. Mojallali, "High step-up isolated dc–dc converter with single input and double output and soft-switching performance for renewable energy applications," *IET Power Electronics*, vol. 12, no. 11, pp. 2942–2952, Sep. 2019, doi: 10.1049/iet-pel.2019.0450.

[7] S. Khosrogorji, M. Ahmadian, H. Torkaman, and S. Soori, "Multi-input DC/DC converters in connection with distributed generation units–A review," *Renewable and Sustainable Energy Reviews*, vol. 66, pp. 360–379, Dec. 2016, doi: 10.1016/j.rser.2016.07.023.

[8] Y. M. Y. Buswig, A. Affam, A.-K. H. bin Othman, N. bin Julai, Y. S. Sim, and W. M. Utomo, "Sizing of a hybrid photovoltaic-hydrokinetic turbine renewable energy system in East Malaysia," in *2020 13th International UNIMAS Engineering Conference (EnCon)*, Oct. 2020, pp. 1–8, doi: 10.1109/EnCon51501.2020.9299329.

[9] L. Solero, A. Lidozzi, and J. A. Pomilio, "Design of multiple-input power converter for hybrid vehicles," *IEEE Transactions on Power Electronics*, vol. 20, no. 5, pp. 1007–1016, Sep. 2005, doi: 10.1109/TPEL.2005.854020.

[10] Y.-F. Wang, L. Xue, C. Wang, P. Wang, and W. Li, "Interleaved high-conversion-ratio bidirectional DC–DC converter for distributed energy-storage systems—circuit generation, analysis, and design," *IEEE Transactions on Power Electronics*, vol. 31, no. 8, pp. 5547–5561, Aug. 2016, doi: 10.1109/TPEL.2015.2496274.

[11] S. S. Dobakhshari, S. H. Fathi, and J. Milimonfared, "High step-up double input converter with soft switching and reduced number of semiconductors," *IET Power Electronics*, vol. 13, no. 10, pp. 1995–2007, Aug. 2020, doi: 10.1049/iet-pel.2019.1394.

[12] Y.-C. Liu and Y.-M. Chen, "A systematic approach to synthesizing multi-input DC-DC converters," *IEEE Transactions on Power Electronics*, vol. 24, no. 1, pp. 116–127, Jan. 2009, doi: 10.1109/TPEL.2008.2009170.

[13] G. Chen, Z. Jin, Y. Deng, X. He, and X. Qing, "Principle and topology synthesis of integrated single-input dual-output and dual-input single-output DC-DC converters," *IEEE Transactions on Industrial Electronics*, vol. 65, no. 5, pp. 3815–3825, May 2018, doi: 10.1109/TIE.2017.2760856.

[14] Y. Li, X. Ruan, D. Yang, F. Liu, and C. K. Tse, "Synthesis of multiple-input DC/DC converters," *IEEE Transactions on Power Electronics*, vol. 25, no. 9, pp. 2372–2385, Sep. 2010, doi: 10.1109/TPEL.2010.2047273.

[15] Y. Yuan-mao and K. W. E. Cheng, "Multi-input voltage-summation converter based on switched-capacitor," *IET Power Electronics*, vol. 6, no. 9, pp. 1909–1916, Nov. 2013, doi: 10.1049/iet-pel.2013.0015.

[16] Y.-M. Chen, A. Q. Huang, and X. Yu, "A high step-up three-port DC-DC converter for stand-alone PV/battery power systems," *IEEE Transactions on Power Electronics*, vol. 28, no. 11, pp. 5049–5062, Nov. 2013, doi: 10.1109/TPEL.2013.2242491.

[17] L.-J. Chien, C.-C. Chen, J.-F. Chen, and Y.-P. Hsieh, "Novel three-port converter with high-voltage gain," *IEEE Transactions on Power Electronics*, vol. 29, no. 9, pp. 4693–4703, Sep. 2014, doi: 10.1109/TPEL.2013.2285477.

[18] V. A. K. Prabhala, P. Fajri, V. S. P. Gouribhatla, B. P. Baddipadiga, and M. Ferdowsi, "A DC–DC converter with high voltage gain and two input boost stages," *IEEE Transactions on Power Electronics*, vol. 31, no. 6, pp. 4206–4215, Jun. 2016, doi: 10.1109/TPEL.2015.2476377.

[19] K. Varesi, S. H. Hosseini, M. Sabahi, and E. Babaei, "Modular non-isolated multi-input high step-up DC–DC converter with reduced normalised voltage stress and component count," *IET Power Electronics*, vol. 11, no. 6, pp. 1092–1100, May 2018, doi: 10.1049/iet-pel.2017.0483.

[20] S. K. Haghighian, S. Tohidi, M. R. Feyzi, and M. Sabahi, "Design and analysis of a novel SEPIC-based multi-input DC/DC converter," *IET Power Electronics*, vol. 10, no. 12, pp. 1393–1402, Oct. 2017, doi: 10.1049/iet-pel.2016.0654.

[21] F. Kardan, R. Alizadeh, and M. R. Banaei, "A new three input DC/DC converter for hybrid PV/FC/battery applications," *IEEE Journal of Emerging and Selected Topics in Power Electronics*, vol. 5, no. 4, pp. 1771–1778, Dec. 2017, doi: 10.1109/JESTPE.2017.2731816.

[22] B. Z. Ghavidel, E. Babaei, and S. H. Hosseini, "An improved three-input DC-DC boost converter for hybrid PV/FC/battery and bidirectional load as backup system for smart home," in *2019 10th International Power Electronics, Drive Systems and Technologies Conference (PEDSTC)*, Feb. 2019, pp. 533–538, doi: 10.1109/PEDSTC.2019.8697731.

[23] R.-J. Wai and B.-H. Chen, "High-efficiency dual-input interleaved DC-DC converter for reversible power sources," *IEEE Transactions on Power Electronics*, vol. 29, no. 6, pp. 2903–2921, Jun. 2014, doi: 10.1109/TPEL.2013.2275663.

[24] J. G. Gorji, K. Abbaszadeh, and F. Bagheroskouei, "A new two-input and multi-output interleaved DC_DC boost converter for satellites power system," in *2019 10th International Power Electronics, Drive Systems and Technologies Conference (PEDSTC)*, Feb. 2019, pp. 236–241, doi: 10.1109/PEDSTC.2019.8697865.

[25] A. M. Al-Modaffer, A. A. Chlaihawi, and H. A. Wahhab, "Non-isolated multiple input multilevel output DC-DC converter for hybrid power system," *Indonesian Journal of Electrical Engineering and Computer Science*, vol. 19, no. 2, pp. 635–643, Aug. 2020, doi: 10.11591/ijeecs.v19.i2.pp635-643.

[26] A. A. Chlaihawi, A. Al-Modaffer, and H. Jedi, "Minimal switching of multiple input multilevel output DC-DC converter," *International Journal of Power Electronics and Drive Systems (IJPEDS)*, vol. 12, no. 2, p. 968, Jun. 2021, doi: 10.11591/ijpeds.v12.i2.pp968-974.

[27] A. Alzahrani, P. Shamsi, and M. Ferdowsi, "An interleaved non-isolated DC-DC boost converter with diode-capacitor cells," in *2017 IEEE 6th International Conference on Renewable Energy Research and Applications (ICRERA)*, Nov. 2017, pp. 216–221, doi: 10.1109/ICRERA.2017.8191269.

BIOGRAPHIES OF AUTHORS

Azuka Affam received the B.Eng. degree in Electrical and Electronic Engineering from Michael Okpara University of Agriculture, Umudike, Nigeria in 2010, and the M.Sc degree in Electronic Systems Design Engineering from Universiti Sains Malaysia in 2017. He is currently pursuing the Ph.D. degree in power electronics and renewable energy integration at Universiti Malaysia Sarawak, Malaysia. His research interests mainly include multi-input DC-DC converters, energy harvesting, renewable energy integration, and battery energy storage systems. He can be contacted at: 18010014@siswa.unimas.my.

Yonis M. Yonis Buswig received his B.Eng. degree from Omar Al-Mukhtar University, Libya, in 2008. The M.Sc. degree in electrical and electronics engineering from Tun Hussein Onn University of Malaysia (UTHM), Batu Pahat, Johor, Malaysia, in 2011. In 2015, he was awarded his Ph.D. degree from Department of Power Engineering, Faculty of Electrical Engineering, Tun Hussein Onn University of Malaysia (UTHM). Currently, he is a Lecturer in the Department of Electrical and Electronic Engineering, Faculty of Engineering, Universiti Malaysia Sarawak. His current research interests include the area of power electronics, renewable energy technology, and motor drives control. He can be contacted at email: byonis@unimas.my.

Al-Khalid Hj Othman graduated his first degree from Nottingham Trent University, U.K in 1995 with BEng. (Hons) in Electrical and Electronic Engineering, followed by MSc. in Information Technology (Digital) from Nottingham University, U.K. in 1996. He obtained his Doctor of Philosophy (Ph.D) in Engineering from Newcastle upon Tyne University, U.K. in 2007 with specialization in Underwater Acoustic Network Protocol. He is a Professor at Faculty of Engineering, Universiti Malaysia Sarawak (UNIMAS). His research interests are communication network protocol and renewable energy. He can be contacted at email: okhalid@unimas.my.

Norhuzaimin Julai received his PhD in Electrical and Electronic Engineering from Newcastle University, UK in 2015. He is with the Department of Electrical and Electronics Engineering, Faculty of Engineering, Universiti Malaysia Sarawak. His research area of interest is in the soft error in integrated circuit (IC), sustainable energy and renewable energy. He is a Chartered Engineer with the Energy Institute UK. He can be contacted at email: jnorhuza@unimas.my.

Hani Albalawi received his BSc degree in electrical engineering from King Abdulaziz University, Jeddah, Saudi Arabia, in 2008, M.S degree in automatic control system engineering from the University of Sheffield, Sheffield, UK, in 2011 and Ph.D. degree from Clemson University, Clemson, SC, USA in 2016. He is a faculty member in Department of Electrical Engineering at the College of Engineering at the University of Tabuk, Tabuk, Saudi Arabia. His research interests include renewable energy, power system quality, power system planning and operation, and power system control. He can be contacted at email: halbala@ut.edu.sa.